Competing exchange interactions and their relevance for the magnetisation process in RMn6-xCrxSn6 powders (with R=Y, Gd, Tb,Dy, Ho, Er)

Brabers, J.H.V.J.; Zhou, G.F.; Colpa, J.H.P.; Buschow, K.H.J.; de Boer, F.R.

DOI
10.1016/0921-4526(94)90179-1

Publication date
1994

Published in
Physica B-Condensed Matter

ELSEVIER

Physica B 202 (1994) 1–10

PHYSICA B

Competing exchange interactions and their relevance for the magnetisation process in $RMn_{6-x}Cr_xSn_6$ powders (R = Y, Gd, Tb, Dy, Ho, Er)

J.H.V.J. Brabers[a,b,*], G.F. Zhou[a], J.H.P. Colpa[a], K.H.J. Buschow[b], F.R. de Boer[a]

[a] *Van der Waals–Zeeman Laboratory, University of Amsterdam, Valckenierstraat 65, 1018 XE Amsterdam, The Netherlands*
[b] *Philips Research Laboratories, P.O. Box 80000, 5600 JA Eindhoven, The Netherlands*

Received in final form 22 December 1993

Abstract

The free-powder magnetisation of $RMn_{6-x}Cr_xSn_6$ compounds has been measured for compounds with R = Y, Gd, Tb, Dy, Ho, Er in fields up to 38 T, and interpreted in terms of a simple model, which is also outlined in this paper. From the measurements, estimates for the R-3d mean-field coupling constant (n_{RT}) could be derived for the cases where R = Gd, Tb, Dy, Ho, Er. In turn, the n_{RT} values can be related to the microscopic spin-coupling constant (J_{RT}). In the case of YMn_6Sn_6 the high-field measurement presents evidence for a very weak antiferromagnetic coupling between the Mn layers. Furthermore, values for the Mn moments (μ_{Mn}) were also derived from the magnetisation measurements. The estimated μ_{Mn} values are of the order of $2.0\mu_B$.

1. Introduction

Recently, Malaman et al. [1–3] have reported on the existence of RMn_6Sn_6 compounds with R = Sc, Y, Gd–Tm, Lu. The crystal structure of these compounds is of the $HfFe_6Ge_6$ type (Pearson symbol hP13, space group number 191). As may be inferred from Fig. 1, this structure can be viewed as consisting of a layered arrangement of R- and Mn-ions in a sequence Mn–R–Mn–Mn–R–Mn. There is only a single crystallographic Mn site. The in-plane Mn–Mn nearest-neighbour distance is about 0.28 nm. The interplane nearest-neighbour Mn–Mn distance is about 0.45 nm. The reported magnetic ordering temperatures of the compounds are above room temperature.

From measurements of the magnetisation versus temperature in the paramagnetic regime it was found that in the compounds with a magnetic R-component, the Mn-ions carry a substantial effective magnetic moment of the order of $3\mu_B$/Mn. In order to investigate the coupling between the different magnetic moments in more detail, we have performed measurements of the free-powder magnetisation of $RMn_{6-x}Cr_xSn_6$ compounds (with R = Y, Gd–Er) as a function of applied magnetic fields up to 38 T.

* Corresponding author.

SSDI 0921-4526(94)00003-E

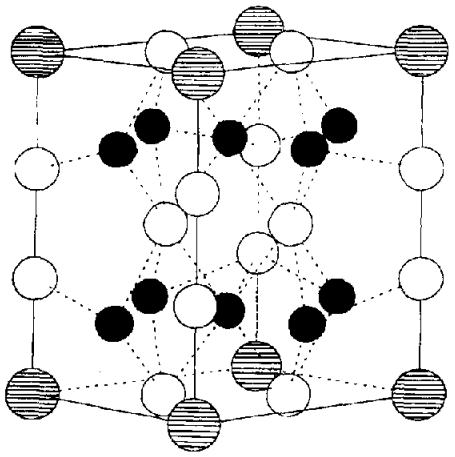

Fig. 1. The $HfFe_6Ge_6$-type unit-cell. The R-ions (shaded) occupy the angular points of the unit-cell. The Mn-ions occupy the black-coloured sites. The layered arrangement of the R- and Mn-ions can be recognised immediately. The Ge-ions are indicated as white circles.

2. Theoretical outline

Some time ago Verhoef et al. [4] have presented a model which supplies a satisfactory explanation of the free-powder magnetisation curves of ferrimagnetic R–Fe and R–Co intermetallics. This model describes the magnetisation process in these compounds in terms of two magnetic sublattices being subject to an interplay between the R–T exchange interaction and the Zeeman energy.

In the model, the anisotropy of the T-sublattice is completely neglected. The powder grains are considered to be single crystalline and free to rotate under the influence of the applied field into their energetically most favourable direction.

At low fields the configuration of the sublattice moments then corresponds to the ferrimagnetic (anti-parallel) alignment. At a certain critical field, however, spin canting occurs: with increasing field the T-sublattice and R-sublattice moment start to rotate continuously towards each other. If the T-sublattice anisotropy is neglected, the R-sublattice moment stays confined to its easy direction during the spin canting. The value of the critical field (B_{cr1}) can be expressed in terms of the mean-field R–T coupling constant (n_{RT}) and the magnitudes of the respective sublattice moments (m_R and m_T) as $B_{cr1} = n_{RT}|m_R - m_T|$. The rotation of the moments continues until at a second critical field $B_{cr2} = n_{RT}(m_R + m_T)$ the ferromagnetic (parallel) alignment is reached. At field values corresponding to a canted spin configuration ($B_{cr1} < B < B_{cr2}$), the relationship between the free-powder magnetisation m and the applied field is linear:

$$m = \frac{B}{n_{RT}}. \tag{1}$$

Using this relation, it is possible to determine an estimate of n_{RT} from the slope of that part of the magnetisation curve that corresponds to the spin canting. This n_{RT} value can then be related to the (microscopic) spin-coupling constant J_{RT} via the following formula [4]:

$$J_{RT} = \frac{-2g_R\mu_B^2 N_T n_{RT}}{(g_R - 1)Z_{RT}}, \tag{2}$$

where g_R represents the g-factor of the R-component, N_T the number of T-ions per mass (or formula) unit, and Z_{RT} the number of nearest T-ion neighbours of an R-ion.

From the outline presented here, it is clear that in the case of ferrimagnetic R–T compounds with T = Fe, Co one can derive information on the strength of the R–T coupling from measurements of the free-powder magnetisation vs B.

One of the basic concepts of the model outlined in the above is the assumption that the interaction between the moments is of the Heisenberg type, and that both R- and T-moments couple together as single sublattices. A behaviour in agreement with the model's description was found in quite a number of R–Fe and R–Co intermetallics [5]. For R–Mn compounds, however, the situation is often different. In many of the R–Mn compounds, the Mn–Mn interaction is of the antiferromagnetic type, and as a consequence, the corresponding compounds with R = Y are pure antiferromagnets. This antiferromagnetic interaction between different Mn moments complicates the description of the (free-powder) magnetisation process in compounds with a magnetic R-component. It is not a priori clear if estimates for n_{RT} can be derived from free-powder magnetisation data in an equally easy and elegant way as in the case of R–Fe and R–Co

compounds. Therefore, a more detailed analysis of the free-powder magnetisation process in R–Mn compounds is necessary.

Anticipating the high-field measurements to be presented later in this paper, we report already here that in RMn_6Sn_6 compounds the Mn–Mn coupling is very weak, and that at low fields the magnetisation values correspond to a collinear ferrimagnetic alignment in the case of magnetic R-ions. For a description of the magnetisation process in compounds with a magnetic R-component, the occurrence of helical spin arrangements can therefore be excluded and the interaction between non-adjacent Mn layers neglected.

Instead of two sublattices, like in Verhoef's model, it is now reasonable to describe the M–B curve within a three-sublattice model. This model describes the magnetisation process in terms of two equivalent Mn-sublattice vectors ($\boldsymbol{m}_{T1}$ and $\boldsymbol{m}_{T2}$) being subject to a mutual interaction of the antiferromagnetic type, and a single R-sublattice vector ($\boldsymbol{m}_R$) coupling to each of the Mn-sublattice vectors.

For a description of the magnetisation process of the three-sublattice system we neglect the Mn anisotropy (following Ref. [4]). The justification for this neglect is that in most R–T intermetallics the T anisotropy is one order of magnitude smaller than the R anisotropy. As a consequence, the R-sublattice moment will remain fixed to its easy direction (or plane), whereas the T moments may change their orientation with respect to the principal magnetic axes when the applied field changes. Therefore, no terms connected with anisotropy effects occur in the free-energy expression connected with the magnetisation process.

To find the most general configuration of the 3 sublattices we consider the vectorial resultant of the applied field and the R–Mn exchange field acting on the Mn sublattices as a single (effective) field $\boldsymbol{B}_{Mn}$. As is common in the case of two sublattices subject to an antiferromagnetic interaction and without anisotropy, the Mn sublattices will align in such a position that $\boldsymbol{B}_{Mn} \neq 0$ is the bisector of the two Mn sublattices. Therefore, the configuration of the two Mn-sublattice magnetisations, and the R-sublattice magnetisation can be represented as in Fig. 2. The special case where the applied field and the R–Mn exchange field cancel ($\boldsymbol{B}_{Mn} = 0$) corresponds to a singular applied field of value $B = n_{RT}m_R$ and will therefore not be discussed here.

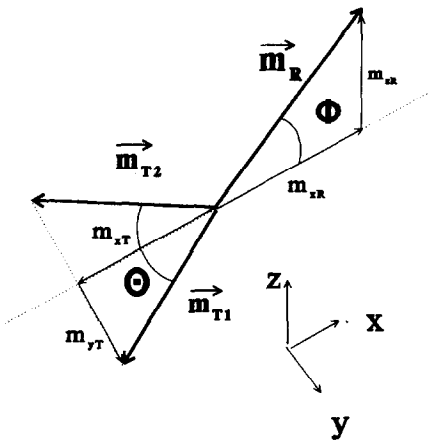

Fig. 2. Model system for R–Mn intermetallics. The Mn-moments couple as two equivalent sublattice magnetisations (m_{T1}, m_{T2}) which are confined to the xy-plane. The R-moments are coupled as one sublattice moment (m_R) confined to the xz-plane. The angles between the Mn sublattice moments are indicated as θ, whereas the angle between the R sublattice moment and the xy-plane is indicated as ϕ.

In the case of single crystalline powder grains which are free to rotate into their energetically most favourable direction, the resultant of the three sublattice magnetisation vectors is parallel to the applied field. For the three-sublattice configuration represented in Fig. 2 the free energy expression then takes the form

$$F = n_{TT}\boldsymbol{m}_{T1}\cdot\boldsymbol{m}_{T2} + n_{RT}\boldsymbol{m}_R\cdot(\boldsymbol{m}_{T1} + \boldsymbol{m}_{T2}) - \boldsymbol{B}\cdot(\boldsymbol{m}_R + \boldsymbol{m}_{T1} + \boldsymbol{m}_{T2}). \quad (3)$$

Here, we have introduced n_{TT} as the mean-field coupling constant corresponding to the Mn–Mn interlayer coupling and n_{RT} as the mean-field coupling constant corresponding to the coupling of one Mn sublattice and the R sublattice. The quantity n_{TT} is related to the spin-coupling constant J_{TT} by a similar expression as given for n_{RT} and J_{RT} in Eq. (2). The only difference is that in the present case, the quantity Z_{RT} has to be replaced by the quantity Z_{TT}: the number of Mn nearest neighbours on the other sublattice. For the quantity N_T, the number of Mn spins per mass unit on one Mn sublattice should be taken instead of the total

number of Mn spins per mass unit. Finally, g_R should be replaced by $g_T = 2$.

To find the equilibrium configuration of the three-sublattice system in an applied field one could now try to minimize the free-energy expression (3) with respect to the angles θ and ϕ indicated in Fig. 2. However, this yields a set of equations that can only be solved by means of a numerical, computational procedure. In order to find an analytic solution of the three-sublattice problem, we therefore present a method based on the equation of motion of a sublattice-magnetisation vector $\boldsymbol{m}_{subl}$ in an effective magnetic field $\boldsymbol{B}_{subl}$:

$$\frac{\partial \boldsymbol{m}_{subl}}{\partial t} = \gamma_{subl}\boldsymbol{\tau}_{subl} = \gamma_{subl}(\boldsymbol{m}_{subl} \times \boldsymbol{B}_{subl}),$$
$$subl = T_1, T_2, R, \tag{4}$$

expressing that $\boldsymbol{m}_{subl}$ is subject to a torque due to the effective field $\boldsymbol{B}_{subl}$. The gyromagnetic ratio γ_{subl} is typical for each sublattice type (R and T). The effective field $\boldsymbol{B}_{subl}$ not only consists of a contribution due to the external field $\boldsymbol{B}$ but also of contributions from the T–T and R–T exchange fields, $\boldsymbol{B}_{T1,2} = -n_{TT}\boldsymbol{m}_{T1,2}$ and $\boldsymbol{B}_{RT} = -n_{RT}\boldsymbol{m}_R$. Every thermodynamical equilibrium configuration, corresponding to a minimum of the energy expression (3), should necessarily be a configuration for which the torque acting on each sublattice magnetisation vector in the three-sublattice system is zero. Our approach will therefore be based on finding all three-sublattice configurations that result in a zero torque on each sublattice. Knowing the vector components of all these sublattice magnetisations, it is then possible to find the free energy connected with each configuration. From all possible configurations, the configuration with the lowest free energy is, of course, the (thermodynamic) equilibrium state. It is stressed that both the cases of positive and negative values of the mean-field parameter n_{RT} can be treated within this approach.

Recognising that in the case of free-powder grains, the total magnetisation $\boldsymbol{m}$ of the three-sublattice system is always parallel to the applied field, two trivial solutions to the zero-torque condition can immediately be derived from Eq. (4): the perfectly anti-parallel alignment and the perfectly parallel alignment of the sublattice moments. However, it is very well possible that there are more types of (canted) sublattice configurations that correspond to a zero torque at a particular value of the applied magnetic field.

In order to find these other configurations, we shall now evaluate the zero-torque condition for the torque $\boldsymbol{\tau}_{T1}$ acting on the Mn-sublattice vector $\boldsymbol{m}_{T1}$. For that purpose, we introduce x, y, z axes as represented in Fig. 2. The Mn sublattices ($\boldsymbol{m}_{T1}$ and $\boldsymbol{m}_{T2}$) are positioned in the xy plane, with the x-axis being defined as the bisector of $\boldsymbol{m}_{T1}$ and $\boldsymbol{m}_{T2}$. The vectors $\boldsymbol{m}_{T1}$, $\boldsymbol{m}_{T2}$, $\boldsymbol{m}_R$, and $\boldsymbol{B}_{T1}$ acting on $\boldsymbol{m}_{T1}$ can be expressed as

$$\boldsymbol{m}_{T1} = \begin{pmatrix} m_{xT} \\ m_{yT} \\ 0 \end{pmatrix}, \quad \boldsymbol{m}_{T2} = \begin{pmatrix} m_{xT} \\ -m_{yT} \\ 0 \end{pmatrix}, \quad \boldsymbol{m}_R = \begin{pmatrix} m_{xR} \\ 0 \\ m_{zR} \end{pmatrix},$$

$$\boldsymbol{B}_{T1} = \begin{pmatrix} B_x - n_{RT}m_{xR} - n_{TT}m_{xT} \\ n_{TT}m_{yT} \\ B_z - n_{RT}m_{zR} \end{pmatrix}, \tag{5}$$

where the fact that $\boldsymbol{B}$ and $\boldsymbol{m}$ are parallel has been incorporated in the expression for $\boldsymbol{B}_{T1}$ (i.e. $B_y = 0$). Substituting these expressions into Eq. (4) and evaluating the vector components of the torque $\boldsymbol{\tau}_{T1}$ acting on $\boldsymbol{m}_{T1}$, one finds for the equilibrium configuration:

$$\boldsymbol{\tau}_{T1} = \begin{pmatrix} m_{yT}(B_z - n_{RT}m_{zR}) \\ -m_{xT}(B_z - n_{RT}m_{zR}) \\ m_{yT}(2n_{TT}m_{xT} + n_{RT}m_{xR} - B_x) \end{pmatrix} = 0. \tag{6}$$

From the vanishing of the x- and y-component of $\boldsymbol{\tau}_{T1}$ follows:

$$\tau_{T1}^2 + \tau_{T1}^2 = (m_{yT}^2 + m_{xT}^2)(B_z - n_{RT}m_{zR})^2$$
$$= m_T^2(B_z - n_{RT}m_{zR})^2 = 0, \tag{7}$$

whence

$$B_z - n_{RT}m_{zR} = 0. \tag{8}$$

The physical interpretation of this expression is that the z-components of the external field and the R–T exchange field acting on $\boldsymbol{m}_{T1}$ have opposite direction, and cancel. From the vanishing of the z-component of $\boldsymbol{\tau}_{T1}$ follows:

$$m_{yT}(2n_{TT}m_{xT} - B_x + n_{RT}m_{xR}) = 0. \tag{9}$$

This expression leaves two possibilities to make the z-component of τ_{T1} vanish:

$$m_{yT} = 0 \text{ or } (2n_{TT}m_{xT} - B_x + n_{RT}m_{xR}) = 0. \quad (10)$$

Because of the symmetry of the spin configuration pictured in Fig. 2, Eqs. (8) and (10) do also correspond to solutions of the zero-torque equation for the sublattice vector $\boldsymbol{m}_{T2}$. Furthermore, the discussion below of the two different solutions represented by Eq. (10) will show that Eqs. (8) and (10) also correspond to solutions of the zero-torque equation for the sublattice vector $\boldsymbol{m}_R$. Therefore Eqs. (8) and (10) can be considered as general conditions to be obeyed by an equilibrium state of the three-sublattice problem.

As the two different solutions of Eq. (10) correspond to entirely different situations, they will be treated separately.

(i) The situation where $m_{yT} = 0$ basically corresponds to the two-sublattice configuration in which both Mn sublattices are parallel to the x-axis ($m_{xT} = \pm m_T$). The case where $m_{zR} = 0$ corresponds to either a ferrimagnetic or a ferromagnetic alignment, whereas the configurations with $m_{zR} \neq 0$ all correspond to a canted spin structure which can be investigated easily as follows.

Since the total magnetisation (m_x, m_y, m_z) should be parallel to the applied field (i.e. $m_x/m_z = B_x/B_z$), the following relations can be obtained:

$$B_x = n_{RT}(m_{xR} + 2m_{xT}) \text{ and } B_y = 0. \quad (11)$$

Combination of these relations and Eq. (8) gives as a result:

$$B^2 = (n_{RT}(m_{xR} + 2m_{xT}))^2 + n_{RT}^2 m_{zR}^2 = n_{RT}^2 m^2 \quad (12)$$

or

$$m = \frac{B}{n_{RT}}, \quad (13)$$

just as expected for the two-sublattice configuration. As stated earlier, such a configuration is a well-known possible equilibrium state for R–Co and R–Fe intermetallics in an applied field [4]. The torques on both the R-sublattice vector and the resultant T-sublattice vector $\boldsymbol{m}_{T1} + \boldsymbol{m}_{T2}$ are zero.

Of course, the solution (13) is only valid in a restricted range of B-values, as the magnetisation is limited to values $|m_R - 2m_T| \leqslant m \leqslant m_R + 2m_T$. Therefore, Eq. (13) may only have any relevance for B-values in the range $n_{RT}|m_R - 2m_T| \leqslant B \leqslant n_{RT}(m_R + 2m_T)$.

(ii) We shall discuss now the case when

$$2n_{TT}m_{xT} + n_{RT}m_{xR} - B_x = 0. \quad (14)$$

As pointed out in the appendix under the reasonable assumption $n_{RT} \neq n_{TT}$, the only case to be discussed is $m_{zR} = 0$, $B_z = 0$. The sublattice configuration corresponding to this case is such that all sublattice magnetisations are confined to the xy plane (Fig. 3(a) and (b)). The resultant T-sublattice moment, the R-sublattice moment, and the applied magnetic field are collinear in this particular configuration, and as a consequence $\boldsymbol{m}_R$ experiences a zero torque just like $\boldsymbol{m}_{T1}$ and $\boldsymbol{m}_{T2}$.

Let the positive x-axis be defined as the direction of the applied field $\boldsymbol{B} = (B,0,0)$, $B > 0$. From Eq. (14) we then have

$$m_{xT} = \frac{-n_{RT}m_{xR} + B}{2n_{TT}} \quad (15)$$

or, considering $m = m_{xR} + 2m_{xT}$, and $m_{xR} = \pm m_R$:

$$m = \frac{\pm(n_{TT} - n_{RT})}{n_{TT}} m_R + \frac{B}{n_{TT}}. \quad (16)$$

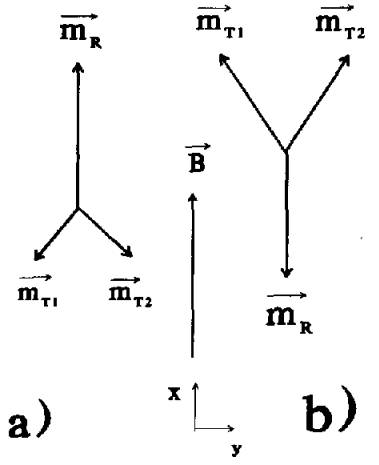

Fig. 3. Sublattice configuration for case (ii). The sublattice moments are all confined to the xy-plane. The cases (a) and (b) correspond to the cases $m_R > 2m_{xT}$ and $m_R < 2m_{xT}$, respectively.

In the right-hand side of Eq. (16) the upper sign corresponds to the case that $\boldsymbol{m}_R$ is parallel to $\boldsymbol{B}$ (Fig. 3(a)), whereas the minus sign corresponds to the case that $\boldsymbol{m}_R$ is antiparallel to $\boldsymbol{B}$ (Fig. 3(b)). Furthermore, it is clear that the configuration considered here can only occur if $n_{TT} > 0$, as Eq. (16) yields a magnetisation which decreases with increasing applied field for $n_{TT} < 0$. The configuration can only have relevance in the cases that Eq. (15) yields a value for m_{xT} such that $|m_{xT}| \leqslant m_T$. As a consequence, the configuration mentioned here can only occur at B-values satisfying $-2n_{TT}m_T \pm n_{RT}m_R \leqslant B \leqslant 2n_{TT}m_T \pm n_{RT}m_R$, as can be derived from Eq. (15).

Eq. (16) describes a straight line, the slope of which is equal to the reciprocal of the n_{TT} coupling constant. At first sight the fact that this slope does not contain any contributions from the R–T coupling may not agree with our intuition. From Figs. 3(a) and 3(b), however, it is clear that in this case the R–T exchange interaction results in a constant field contribution (anti)parallel to the external field. Therefore, the R–T exchange interaction does not contribute to the slope. The only effect arising from it is a canting of both T moments already at zero applied field.

Summarizing the theoretical outline so far, we see that the zero-torque condition yields four possible candidates for the equilibrium state: the anti-parallel (ferrimagnetic) alignment (I), the parallel (ferromagnetic) alignment (II), the canted quasi- two-sublattice configuration (III), and the three-sublattice configuration with all sublattice moments confined to the xy-plane (IV), as displayed in Fig. 3. From the above, sufficient information on the vector components of the three sublattices can be derived for each configuration to write down the free-energy expression for each case:

$$F_I = n_{TT}m_T^2 - 2n_{RT}m_Rm_T - B|m_R - 2m_T|, \qquad (17a)$$

$$F_{II} = n_{TT}m_T^2 + 2n_{RT}m_Rm_T - B(m_R + 2m_T), \qquad (17b)$$

$$F_{III} = n_{TT}m_T^2 - \frac{n_{RT}}{2}(m_R^2 + 4m_T^2) - \frac{B^2}{2n_{RT}}, \qquad (17c)$$

$$F_{IV} = \frac{-n_{RT}^2m_R^2 - 2n_{TT}^2m_T^2}{2n_{TT}} \pm \frac{n_{RT}m_R - n_{TT}m_R}{n_{TT}}B - \frac{B^2}{2n_{TT}}. \qquad (17d)$$

For a given set of the parameters n_{RT}, n_{TT}, m_T, m_R, and the applied field B, the equilibrium configuration corresponds to the configuration with the lowest value for the free energy following from Eqs. (17), under the constraint that $|m_R - 2m_T| < m < |m_R + 2m_T|$ (in the case of Eq. (17c)), and $|m_{xT}| \leqslant m_T$ (in the case of Eq. (17d)). This competition between the different sublattice configurations corresponding to Eqs. (17a)–(17d) may result in magnetic phase transitions connected with transitions from one configuration into another. An elaborate discussion of the various possible phase transitions will be given in a forthcoming paper [6].

3. Experimental

$RMn_{6-x}T_xSn_6$ compounds (with R = Y, Gd, Tb, Dy, Ho, Er, and T = Cr; for the values of x, see below) were prepared by arc melting stoichiometric mixtures of the metallic constituents of at least 99.9% purity. After arc melting, the polycrystalline specimens were wrapped in tantalum foil, sealed into evacuated quartz tubes and annealed at 700°C for 10 days or more. After this, they were cooled to room temperature within half an hour. After this treatment, the samples were investigated by X-ray powder diffraction and found to be approximately single phase. The X-ray patterns were indexed on the basis of the $HfFe_6Ge_6$-type structure (space group P6/mmm (no. 191), Pearson symbol hP13). Data on the free-powder magnetisation as a function of the applied magnetic field up to 38 T were obtained for each compound at 4.2 K in the high field Installation of the University of Amsterdam [7].

4. Results and discussion

Figs. 4(a)–(f) represents the high field measurements on the free-powder magnetisation of the

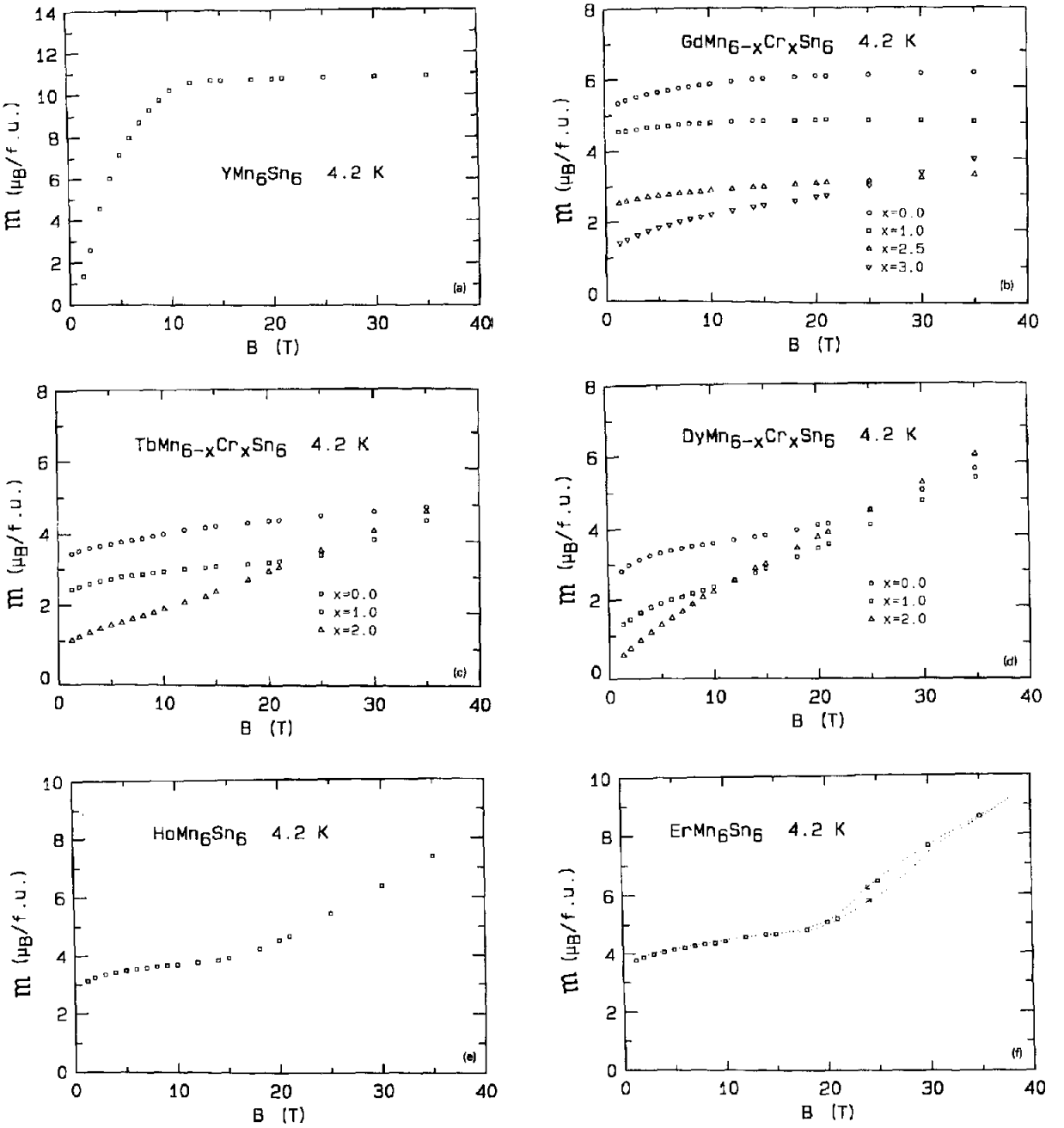

Fig. 4. High field magnetisation measurements for $RMn_{6-x}Cr_xSn_6$ compounds with R = Y, Gd, Tb, Dy, Ho, Er.

$RMn_{6-x}Cr_xSn_6$ compounds (with R = Y, Gd, Tb, Dy, Ho, Er).

The data for YMn_6Sn_6 are shown in Fig. 4(a). In the low-field part of the curve shown in Fig. 4(a), the magnetisation m is a roughly linear function of the applied field B. At an applied field strength of about 10 T the magnetisation reaches saturation, and remains constant at field values beyond 10 T.

As YMn_6Sn_6 is a pure antiferromagnet with a Néel temperature of 333 K [2], and preliminary neutron diffraction experiments [3] have shown evidence for a helical arrangement of Mn-spins in this compound, the steep linear increase of the magnetisation with the applied field below 10 T can be interpreted as a rotation of the magnetisation vectors of the Mn sublattices towards a direction parallel to $\boldsymbol{B}$. At $B \simeq 10$ T these magnetisation vectors reach a parallel (ferromagnetic) alignment which persists at higher B-values. The (saturated) value of the magnetisation is $10.5\mu_B$ per formula unit, which corresponds to a magnetic moment of $1.75\mu_B$ per Mn-ion.

Due to the helical Mn-spin arrangement, the data presented in Fig. 4(a) cannot be analysed in terms of the two- or three-sublattice model mentioned previously in this paper. The effect of such a helical spin configuration on the magnetisation curve is still subject of investigation and therefore no estimate for the mean-field interlayer coupling constant can be presented within the scope of the present paper. However, the magnetisation reaches saturation at quite low fields already, suggesting that the coupling between the Mn layers is very weak.

In Figs. 4(b)–(e) high field magnetisation data are shown for $RMn_{6-x}Cr_xSn_6$ compounds, with R = Gd, Tb, Dy, and Ho, respectively. It is reasonable to assume that for these particular compounds a description in terms of the three-sublattice model presented earlier in this paper is justified and that a helix-like configuration of the Mn spins is absent. The main argument for this may be found in the very small Mn inter-layer coupling revealed by the data presented in Fig. 4(a) for YMn_6Sn_6 and the values of the magnetisation at low fields which corresponds to a collinear ferrimagnetic alignment in all cases.

In the cases where R = Gd and $x = 0$, 1, 2.5, or R = Tb and $x = 0$, the magnetisation shows a tendency towards saturation for the higher fields in the B-interval up to 35 T. The other curves in Figs. 4(b)–(e), however, display a kink at some critical field B_{crit}, beyond which the magnetisation increases linearly with the applied field. Provided that the Mn-ions have moments of about $2\mu_B$/Mn, at low fields the magnetisation measured is in accordance with the situation that the Mn moments point in the direction of the applied field and the R-moments and the Mn-moments are antiparallel. For this reason we exclude the possibility of some helical arrangement of the Mn-moments, and we assume that the three-sublattice model is applicable. A transition at B_{crit} to the configuration with the magnetisation of the three sublattices pointing in three different directions, i.e. the R-moments still antiparallel to the applied field and the bisector of the Mn-moments in the direction of this field, can be excluded. This is because a small non-zero angle between the Mn-moments would imply an increase of the Zeeman as well as the total exchange contribution to the free energy. (At zero field, in which only exchange coupling plays a role, we derive from the magnetisation measured, that the antiparallel configuration is the energetically most favourable one.) Therefore, the linear increase of m with B displayed by the curves in Figs. 4(b)–(e) with a kink should be seen as a result of a canting within the quasi- two-sublattice configuration (R and Mn) rather than within the three-sublattice configuration just considered. In the quasi- two-sublattice picture, the Mn spins are coupled together as one sublattice, and beyond B_{crit} the R- and Mn-moments rotate towards each other with increasing B-value. The slope of that part of the magnetisation curve connected with the spin canting should, in agreement with Eq. (13), be proportional to the inverse of the n_{RT} coupling constant and free from contributions from the Mn–Mn interaction. The fact that we did not find a critical field for some compounds as discussed above, agrees with our expectation that for low Cr concentration (high T-moment) the critical field lies well above the fields used in our experiments.

The main difference between the experimental data and the predictions based on the three-sublattice model, is that, according to theory, the magnetisation should be a constant below the critical field B_{crit} whereas the experimental data show a (small) slope also below B_{crit}. Such phenomena have also been observed for other R–T compounds in which the T-sublattice is simply ferromagnetic. This slope of the low field part of the curve increases slightly with increasing Cr concentration and is still a subject of investigation. A possible explanation

may be found in the dilution of the Mn sublattice by substitution of Mn-ions with Cr-ions. (In $RMn_{6-x}Cr_xSn_6$ compounds the Cr-ions carry no magnetic moments or moments which are at least smaller than the Mn moments. As an indication for this we mention the decrease of the critical field $B_{crit} = n_{RT}|m_R - 2m_T|$ with increasing Cr concentration as observed in Figs. 4(b)–(e).) The Cr-ions disturb the magnetic structure on a microscopic scale, and might favour a rotation of a few Mn spins already at fields in which the rest of the Mn moments still keep their orientation anti-parallel to the R-moments.

In Fig. 4(f), the measured free-powder magnetisation of $ErMn_6Sn_6$ is presented as a function of the applied field. The data points marked by the open squares correspond to measurements in a decreasing magnetic field, where for each measuring point this field has been kept constant for a few milliseconds. The dotted curve corresponds to measurements in a field increasing linearly with time to a maximum value (38 T) and then decreasing linearly with time back to zero. The dots mark the individual datapoints.

Probably the most dominant feature of the dotted curve is the hysteresis loop between 20 T and 35 T. We have no well-based explanation for this effect. One possibility is that, like in other Er–T intermetallics [5], the Er moments couple together not as one but as a few different sublattice vectors, all confined to the basal plane. A reorientation of the Er sublattice moments with increasing field may then cause the observed hysteresis. Still, the main contribution to the observed slope beyond 20 T arises from a canting of the Mn sublattice towards the resultant Er moment.

Estimates for the n_{RT} coupling constant were derived from the slopes of the linear high field parts of the curves presented in Fig. 4(b)–(f). With the use of Eq. (2) the obtained n_{RT} values can be related to values for the J_{RT} spin coupling constants. Both the n_{RT}- and the related J_{RT}/k-values (where k is Boltzmann's constant) are listed in Table 1 ($Z_{RT} = 12$). The values for $ErMn_6Sn_6$ should be taken with some reservation, as they are not very accurate due to the hysteresis in the magnetisation curve.

The high field measurements also provide information on the Mn moments in the different compounds. As mentioned before, from the saturation magnetisation m_s of YMn_6Sn_6, a magnetic moment of 1.75 μ_B per Mn ion can be derived. In the case of compounds with a magnetic R component, a value for m_s can be obtained by extrapolation of the magnetisation curve before $B = B_{crit}$ to $B = 0$. From the m_s values found in this procedure, an estimate can be obtained for the Mn moments, assuming the Cr-moments to be zero and the R-moments to be equal to the corresponding free-ion

Table 1
R–Mn coupling constants, saturation magnetisation and Mn-moments of the $RMn_{6-x}Cr_xSn_6$ compounds investigated

Compound	n_{RMn} (T f.u./μ_B)	J_{RMn}/k (K)	m_s (μ_B/f.u.)	μ_{Mn} (μ_B/ion)
$GdMn_6Sn_6$	–	–	5.9	2.2
$GdMn_5CrSn_6$	–		4.7	2.3
$GdMn_{3.5}Cr_{2.5}Sn_6$	–	–	2.7	2.8
$GdMn_3Cr_3Sn_6$	13.17	− 8.85	1.7	2.9
$TbMn_6Sn_6$	–	–	3.7	2.1
$TbMn_5CrSn_6$	10.43	− 10.45	2.7	2.3
$TbMn_4Cr_2Sn_6$	9.29	− 9.36	0.9	2.5
$DyMn_6Sn_6$	8.42	− 11.31	3.1	2.2
$DyMn_5CrSn_6$	7.62	− 10.24	1.4	2.3
$DyMn_4Cr_2Sn_6$	6.63	− 8.91	0.5	2.5
$HoMn_6Sn_6$	5.16	− 8.67	3.3	2.2
$ErMn_6Sn_6$	5.11	− 10.30	3.9	2.2
YMn_6Sn_6	–	–	10.5	1.75

moments. The values for the magnetic moments per Mn ion, related to the observed m_s values are also listed in Table 1. The value for $GdMn_3Cr_3Sn_6$ should be taken with some reservation as it is unlikely high. A remarkable phenomenon is the substantial difference between the Mn moment in YMn_6Sn_6 and the Mn moments in the compounds with a magnetic R-component. This suggests that in the latter case the R-moments induce an extra contribution to magnetic moments on the Mn ions. This phenomenon has also been observed earlier in many R–Co intermetallics (see for instance Ref. [8]).

A comparison of the J_{RT}/k-values listed in Table 1 with values found in R_2Fe_{17}, R_2Co_{17}, and $R_2Fe_{14}B$ [9], shows only small differences. The J_{RT}/k-values listed in Table 1 are of the order of 9.5 K, whereas for R_2Fe_{17} and R_2Co_{17} the values are of the order of 7 K, and for $R_2Fe_{14}B$ of the order of 8.5 K. Future investigations will deal with the concentration dependence of the J_{RMn} coupling constant, to establish whether J_{RMn} decreases with the T-ion concentration, analogous to the cases with T = Co,Fe [9].

Appendix: Solution for the case where $m_{zR} \neq 0$

Considering that $\boldsymbol{B}$ and $\boldsymbol{m}$ are parallel, and that according to Eq. (8), $B_z = n_{RT} m_{zR}$, we have for a case where $m_{zR} \neq 0$:

$$\frac{m_{xR} + 2m_{xT}}{m_{zR}} = \frac{m_x}{m_z} = \frac{B_x}{B_z} = \frac{B_x}{n_{RT} m_{zR}}$$

so that we have

$$B_x = n_{RT}(m_{xR} + 2m_{xT}). \tag{A1}$$

Using Eq. (14), a second expression for B_x can be obtained:

$$B_x = n_{RT} m_{xR} + 2n_{TT} m_{xT}. \tag{A2}$$

Equating (A1) and (A2) yields

$$n_{RT} m_{xR} + 2n_{RT} m_{xT} = n_{RT} m_{xR} + 2n_{TT} m_{xT}. \tag{A3}$$

As in general $n_{RT} \neq n_{TT}$, Eq. (A3) can only hold if $m_{xT} = 0$. This means (see Fig. 2) that $\boldsymbol{m}_{T1}$ and $\boldsymbol{m}_{T2}$ are antiparallel. The applied field is parallel to $\boldsymbol{m}_R$.

The case where $\boldsymbol{m}_{T1}$ and $\boldsymbol{m}_{T2}$ are antiparallel implies a configuration where $\boldsymbol{m}_R$ is perpendicular to the alignment axis of $\boldsymbol{m}_{T1}$ and $\boldsymbol{m}_{T2}$. It is clear that $\boldsymbol{m}_R$ is not unique in this case: every vector $\boldsymbol{m}_R$ positioned in the xz-plane corresponds to a proper solution. However, it is easy to verify that all the solutions $m_{zR} \neq 0, m_{xT} = 0$ are equivalent to a solution where $m_{zR} = 0$ and $m_{xT} = 0$. This is just a special case of the three-sublattice configuration discussed earlier. Therefore, we conclude that no separate discussion of the case $m_{zR} \neq 0$ is necessary.

References

[1] B. Malaman, G. Venturini and B. Roques, Mater. Res. Bull. 23 (1988) 1629.
[2] G. Venturini, B. Chafik El Idrissi and B. Malaman, J. Magn. Magn. Mater. 94 (1991) 35.
[3] B. Chafik El Idrissi, G. Venturini and B. Malaman, J. Less-Common Met. 175 (1991) 143.
[4] R. Verhoef, F.R. de Boer, J.J.M. Franse, C.J.M. Denissen, T.H. Jacobs and K.H.J. Buschow, J. Magn. Magn. Mater. 83 (1990) 139.
[5] R. Verhoef, Thesis, University of Amsterdam (1990).
[6] J.H.P. Colpa and J.H.V.J. Brabers, to be published.
[7] R. Gersdorf, F.R. de Boer, J.C. Wolfrat, F.A. Muller and L.W. Roeland, in: High-Field magnetism, ed. M. Date (North-Holland, Amsterdam, 1983) p. 277.
[8] J.P. Liu, F.R. de Boer and K.H.J. Buschow, J. Less-Common Met. 175 (1991) 137.
[9] F.R. de Boer and K.H.J. Buschow, Physica B 177 (1992) 199.